First-Principle Modelling of Forsterite Surface Properties: Accuracy of Methods and Basis Sets

Raffaella Demichelis*†, Marco Bruno‡, Francesco R. Massaro§, Mauro Prencipe¶, Marco De La Pierre‖, Fabrizio Nestola**

April 24, 2015

Abstract

The seven main crystal surfaces of forsterite (M_g2SiO_4) were modeled using various Gaussian-type basis sets, and several formulations for the exchange-correlation functional within the Density Functional Theory (DFT). The recently developed pob-TZVP basis set provides the best results for all properties that are strongly dependent on the accuracy of the wavefunction. Convergence on the structure and on the BSSE-corrected surface energy can be reached also with poorer basis sets. The effect of adopting different DFT functionals was assessed. All functionals give the same stability order for the various surfaces. Surfaces do not exhibit any major structural differences when optimized with different functionals, except for higher energy orientations where major rearrangements occur around the Mg sites at the surface or sub-surface. When dispersions are not accounted for, all functionals provide similar surface energies. The inclusion of empirical dispersions raises the energy of all surfaces by a nearly systematic value proportional to the scaling factor s of the dispersion formulation. An estimation for the surface energy is provided through adopting C_6 coefficients that are more suitable than the standard ones to describe O-O interactions in minerals. A 2x2 supercell of the most stable surface (010) was optimized. No surface reconstruction was observed. The resulting structure and surface energy show no difference with respect to those obtained when using the primitive cell. This result validates the (010) surface model here adopted, that will serve as a reference for future studies on adsorption and reactivity of water and carbon dioxide at this interface.

*Electronic address: raffaella.demichelis@curtin.edu.au; Corresponding author

†Nanochemistry Research Institute, Curtin Institute for Computation, and Department of Chemistry, Curtin University, GPO Box U1987, Perth, WA 6845, Australia

‡Dipartimento di Scienze della Terra, Università degli Studi di Torino, Via Valperga Caluso 35, 10125 Torino, Italy

§Dipartimento di Geoscienze, Università degli Studi di Padova, Via Gradenigo 6, 35131 Padova, Italy

¶Dipartimento di Scienze della Terra, Università degli Studi di Torino, Via Valperga Caluso 35, 10125 Torino, Italy

‖Nanochemistry Research Institute, Curtin Institute for Computation, and Department of Chemistry, Curtin University, GPO Box U1987, Perth, WA 6845, Australia

**Dipartimento di Geoscienze, Università degli Studi di Padova, Via Gradenigo 6, 35131 Padova, Italy

Keywords: olivine, forsterite, surface crystallographyc orientation, surface energy, dispersion interactions, DFT

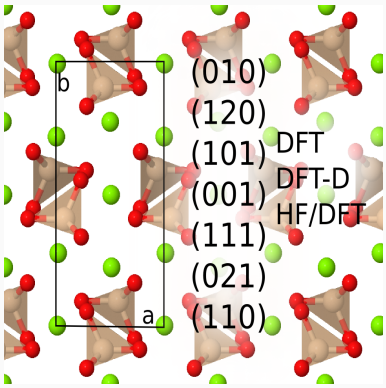

This paper presents an accurate assessment of methods for the study of forsterite surface properties and reactivity. The ability to build a realistic model for such system is essential to understand the fundamental interactions responsible for a variety of natural phenomena happening on Earth and in space.

INTRODUCTION

Olivines ($M_1M_2SiO_4$, with M_1 and M_2 being divalent cations, most frequently Mg^{2+} and/or Fe^{2+}) are major components of the Earth upper mantle and of many extra-terrestrial planetary bodies. As a consequence, they are also involved in the majority of the chemical phenomena occurring on Earth and in space.[1–5]

While much research has been devoted to determine and understand the bulk properties of olivines, especially of those containing iron and magnesium,[6–11] little attention has been devoted to investigate their surfaces, which are indeed the *locus* where chemical reactions take place.

In this context, a main challenge is understanding the mechanisms by which geochemical reactions occur at the olivines/water interface, especially now that a natural high pressure polymorph of $(Mg,Fe)_2SiO_4$ has been found for the first time, showing an extremely high hydration.[12] A second main challenge is learning how to exploit these reactions on a large scale to produce hydrogen and to store carbon dioxide.[1,2,5,13–15] From a broader interdisciplinary perspective, a full understanding of the physical and chemical details that are at the basis of the interaction of olivine surfaces with water or other solid (*e.g.* diamond) and fluid (*e.g.* CO_2) materials would certainly contribute to achieve a better knowledge of abiogenetic processes and planetary evolution.[16,17]

In recent years, a number of papers have appeared, tackling the complex task of developing models able to provide a reliable description of the atomic details of this mineral interface.[18–31] Most of these studies focus on the interaction of hydrogen, water or carbon dioxide with the (010) surface of forsterite (where both M sites are occupied by magnesium) as modeled either with interatomic potentials,[19,24] or with first-principle methods based on the Density Functional Theory (DFT).[25,27,30,31] Of the latter, one presents a study on the adsorption of H_2 molecules on the (010) surface of forsterite performed at the hybrid meta-GGA (Generalized Gradient Approximation) level of theory, though structures were optimized by using interatomic potentials;[27] four deal with the adsorption of either water molecules or H atoms and H_2 molecules on the same surface, simulated at the GGA[25,28,31] and B3LYP-D*[30] levels. Very recently, a GGA study on the adsorption of water molecule on the (100) surface

has also been published.[26]

The remaining main surfaces of forsterite have been partly or fully considered in three studies, two of which applying force field models[18,20] and one, by the present authors, applying hybrid GGA functionals.[32] The investigations by Watson et al.[20] and by Bruno et al.[32] provide a quite comprehensive characterization of the energy and morphology of forsterite surfaces in vacuum. The next step would be developing models able to make realistic predictions regarding the structural and energetic details of their interactions with water and other solid and fluid materials as a function of the cation distribution. Due to the complexity of these processes (which include nucleation and dissolution, electron transfer, physical and chemical adsorption) the development of both force field and first-principle models is extremely important. However, as mentioned above, this task has only been partly addressed for the (010) and (100) surfaces and without providing much detail on the accuracy of the adopted computational methodology in the majority of the cases.

In this paper we present a critical assessment of the accuracy of some of the most widely adopted DFT schemes, including hybrid functionals and empirical dispersions schemes, in describing the structural and energetic properties of forsterite surfaces. Gaussian type basis sets of different quality have also been considered, including those recently developed by Peintinger et al.[33], which allow increasing the accuracy of solid state calculations at a triple-zeta split valence level. Since surface reconstruction has been observed in many surfaces,[32] a supercell model for the most stable surface (010) is here investigated as well.

METHODOLOGY

All the calculations were performed with CRYSTAL14,[34] a periodic *ab initio* package implementing both DFT and Hartree-Fock (HF) methods and using Gaussian-type basis sets.

Four different all-electron basis sets were tested, three of which originally optimized for pyrope[35] ($Mg_3Al_2(SiO_4)_3$) and one recently developed by Peintinger et al.[33] for solid state systems in general. Their accuracy in predicting crystal and surface properties of forsterite is described in the following section. The Basis Set Superposition Error (BSSE), disregarded in a previous study by the present authors, was included according to the counterpoise

correction scheme proposed by Boys and Bernardi.[36] In particular, layers of ghost atoms have been added to the surfaces until convergence at the second digit on surface energy was reached (10^{-2} J m^{-2}).

The effect of several exchange-correlation functionals on the surface energy and morphology of forsterite was tested. In particular, PBE,[37] its revised version for solids (PBEsol[38]) and its corresponding hybrid version (PBE0[39]) were adopted, along with the popular B3LYP[40–42] hybrid functional. Empirical long-range corrections for van der Waals interactions, as proposed by Grimme (B3LYP-D2,PBE-D2),[43,44] were also applied. Results are discussed in a following section.

Thresholds controlling the accuracy of the Coulomb and HF exchange series were set more strictly than default values (TOLINTEG 8 8 8 8 18, see Ref.[45] for further details). Thresholds that control the bipolar approximation of Coulomb bielectronic integrals were tightened too (to 10^{-18}).[45] The threshold on the Self Consistent Field energy was set to 10^{-8} hartree for all but vibrational frequency calculation, where the threshold was set to 10^{-10} hartree.

The remaining computational parameters were set as in Bruno et al.[32], as well as the same geometry optimization scheme was adopted. Vibrational frequencies were obtained within the harmonic approximation, through diagonalization of the dynamical matrix computed by central finite differencing of the analytic gradients with respect to atomic Cartesian coordinates. Elastic constants were obtained by computing the numerical second derivatives of the energy with respect to the strain along each Cartesian direction, as implemented by Erba, Perger and co-workers[45–47]. Four deformations have been applied for each independent strain matrix by varying the dimensionless strain amplitude in steps of of 0.01, in order to estimate the numerical second derivatives. The electronic high frequency components of the dielectric tensor were computed through a Coupled-Perturbed Kohn-Sham method, as described in Ref.[45] and references therein.

The slab model Two-dimensional slabs were created starting from the optimized structure of forsterite. Surfaces were cut according to Hart[48], as discussed in a previous paper.[32]

Surface energies γ [J m^{-2}] at 0 K were obtained as follows:

$$\gamma = \lim_{n\to\infty} E_s(n) = \lim_{n\to\infty} \frac{E_{slab}(n) - nE_{bulk}}{2A} \quad (1)$$

where $E_{slab}(n)$ and E_{bulk} are the energy of an n-layer slab and of the bulk, respectively; A is the area of the surface unit cell; the factor 2 accounts for the upper and lower surfaces of the slab model.

The thickness of the slab (i.e. the number of d_{hkl} layers) was set as in Bruno et al.[32], so that the relative difference between $E_s(n)$ and $E_s(n-1)$ is $< 1\%$.

RESULTS AND DISCUSSION

Basis Sets and Basis Set Superposition Error

Four different all-electron Gaussian-type basis set were used. Three of them, called BS1, BS2 and BS3 from now on, were originally optimized for pyrope,[35] and BS2 was then applied in a number of successful studies on other silicates, including olivines (*e.g.* Refs.[49–51]). This basis set consists of the following contraction: (8s)-(511sp)-(1d) for magnesium, with the exponents of the most external sp and d shells being 0.2245 and 0.5 bohr^{-2}, respectively; (8s)-(411sp)-(1d) for oxygen, with exponents 0.2505 (outer sp) and 0.5 (d) bohr^{-2}; and (8s)-(6311sp)-(1d) for silicon, with exponents 0.13 (outer sp) and 0.6 (d) bohr^{-2}. A basis set similar to BS2 was adopted in Ruiz-Navarro et al.[30], though a more accurate contraction was used for magnesium atoms in the first layer, in order to describe with accuracy the interactions with the adsorbed species at a reduced computing cost.

To check the convergence of the BS2 contraction with the properties of interest (structure, surface energy), calculations have been repeated with one poorer and one richer contractions, namely BS1 and BS3, respectively. The former is the same as BS2 for Mg and O, but has only one sp polarization shell on Si, with exponent 0.322 bohr^{-2}. The latter is the same as BS2 for Mg, but adds a further d shell to both O and Si, with the exponents (again optimized for pyrope) being 2.0 and 0.41 bohr^{-2} for the d shells on O, and 2.56 and 0.54 bohr^{-2} for the d shells on Si.

The fourth basis set is that recently developed by Peintinger and co-workers.[33] It consists of a TZVP contraction that has been systematically derived for solid state systems starting from def2-TZVP[52,53] basis sets devised for molecular cases, and it is denoted as pob-TZVP.

Table 1 reports a comparison of bulk and surface properties of forsterite obtained with the B3LYP functional and the four basis sets (the last three columns will be commented in the next Sections). The latter can all be considered equally accurate to reproduce the structural features of both the bulk and the (010) surface (an overestimation of volumes by 2-3% is mostly due to the adopted functional). Within the BS1-3 series, a clear improvement of vibrational, elastic, and dielectric properties of bulk forsterite is observed when adopting BS2, due to the better description of the strongly covalent Si-O bonds. This is in agreement with Ruiz-Navarro et al.[30], who found that accurate results can be obtained for the (010) surface through performing calculations with a BS2-type basis set on structures optimized with a poorer basis set. Data in Table 1 show also no significant improvement when using a richer basis set of the same series (BS3).

Minor improvements are observed on the prediction of vibrational and elastic properties of forsterite when pob-TZVP is used. As also observed for α-quartz in Maschio et al.[54], this basis set provides better predictions of dielectric properties, and is expected to provide better results in the calculation of any property that requires a very accurate description of the wavefunction. However, the drawback is an increase in computing time by a factor $\frac{t_{pob-TZVP}}{t_{BS2}} \simeq 2$ on forsterite with respect to BS2. Table 1 shows that this point can become important in surface calculations, where multiple-layer supercells with low or no symmetry are involved ($\frac{t_{pob-TZVP}}{t_{BS2}} \simeq 3$ in the selected case).

Surface energy values calculated with the four basis sets and corrected by BSSE (not considered in our previous work, where BS2 was adopted[32]) are also reported in table 1 for the (010) surface. As expected, estimations obtained using more accurate basis sets are affected by a lower BSSE error. Notably, when considering surface energies the effect of BSSE correction is much more important than the choice of the basis set. Table 2 shows that correcting our previous results[32] by the BSSE leads to surface energies that are on average 26% lower when using BS2, and that they almost coincide with those obtained with pob-TZVP (where on average the BSSE correction is 12%). Most importantly, the relative

energy of the various surfaces remains unchanged with respect to our previous predictions.

Despite BS2 can be considered a good compromise between accuracy and computing costs for the prediction of structure and directly related properties (e.g.. vibrational and elastic properties), pob-TZVP turns out to be a better choice for calculating properties that show a stronger dependence on the basis set. As a matter of facts, pob-TZVP has distinct optimized exponents for s and p valence shells, and has been systematically derived from the well-tested def2-TZVP molecular basis sets. However, whereas BS2-type basis sets are the results of 30 years of basis set development and optimization for minerals and have been successfully adopted in tens of studies,[45] pob-TZVP basis set for solid state is quite recent, and therefore it has been tested on a limited number of systems and properties. In this section we have shown that pob-TZVP is at present one of the most accurate options to model surface properties of Mg-olivine, and therefore in the following sections we will present results obtained with this basis set only.

Results obtained on geometries suggest that in future applications on adsorption and reactivity, where the computing time could represent a limit for the feasibility of calculations and, at the same time, an accurate basis set is required to describe the interface, a combined basis set could be used: pob-TZVP can be applied on atoms at the surface, and BS2 on bulk atoms. A similar approach, originally suggested by Civalleri and co-workers,[55,56] has been partly applied by Ruiz-Navarro et al.[30], where Mg atoms at the surface, responsible for the interactions with hydrogen, where described with a more accurate basis set with respect to the rest of the atoms. This, added to the fact that geometry optimization can be confidently performed with BS2, would drastically reduce the amount of resources required to perform such calculations.

Effect of the Hamiltonian

Motivated by several studies that show systematic errors affecting DFT functionals,[50,51,57–60] especially when dealing with thermodynamic predictions, we have performed geometry optimization for all the considered surfaces with various DFT functionals and the pob-TZVP basis set, including GGA-type functionals and hybrid functionals. The effect of including the empirical correction for dispersions as proposed by Grimme[44] is also investigated.

Surface Energy

Table 3 shows surface energies obtained with the various DFT schemes. Pure GGA and hybrid functionals provide very similar values for γ, with differences of $\pm$ 0.1 J m^{-2}. Most importantly, the stability order of the various surfaces remains unchanged. The only exceptions are surfaces (001) and (101), which can be considered almost isoenergetic as their energy difference is in the order of 0.01 J m^{-2}. On average, γ obtained with PBE and B3LYP, which tend to overestimate lattice parameters and bond lengths, are slightly lower than those obtained with PBEsol and PBE0, as a result of slightly weaker interactions between neighbours that overstabilise the surface with respect to the solid.

To the best of our knowledge, the effect of dispersion interactions in describing surface properties of minerals has never been investigated, though studies[30,61–64] applying DFT-D2[44] or alternative methods[63,65] to investigate adsorption of molecules and atoms on mineral, metal and metal oxide surfaces are present in the literature.

As documented in table 3, γ increases by 20 to 40% when applying B3LYP-D2 and PBE-D2 functionals. In particular, this increase is almost systematic, by about 0.3 (PBE-D2) and 0.4-0.5 (B3LYP-D2) J m^{-2}. This is not surprising: dispersion forces are expected to stabilise the solid more than its surfaces, as they depend on the number of neighbours which is lower for surface atoms. However, the main challenge here is understanding whether such an increase is realistic or not, and why the two dispersion corrected functionals provide values that are systematically different.

Since PBE and B3LYP functionals provide approximately the same values for γ, the difference between the results obtained with PBE-D2 and with B3LYP-D2 can be fully attributed to dispersion interactions. In particular, the scaling parameter, s, which multiplies the dispersion energy by 1.05 in B3LYP-D2 and by 0.75 in PBE-D2, can be considered the main responsible for such difference.

It is well known that a certain level of arbitrariness is present when calculating dispersion contributions in solids using the D2 scheme. The parametrization that is usually adopted was proposed by Grimme[44] on the basis of accurate calculations on a range of molecules, dimers, and small clusters. However, as already pointed out in a series of studies,[58,59,63,66] the

dispersion coefficients strongly depend on atomic polarizability, which is extremely sensitive to the local environment of an atom. The more atomic polarizabilities deviate from the molecular cases considered by Grimme, the more dispersion energy deviates from a realistic prediction.

For example, according to Grimme's parameters, Si-Si, Si-Mg and Mg-Mg interactions should dominate the dispersion corrections (C_6^{Mg} = 59.18, C_6^{Si} = 95.66 eV Å^6) whereas oxygen atoms are expected to give a negligible contribution ($C_6^O = 7.25eV$ Å^6). This is very different from what is generally assumed for olivines, where both magnesium and silicon have formal charge around +2 $|e|$, and oxygen assumes a charge between -1 and -2 $|e|$ (in forsterite it is -1.4 $|e|$ on average, using B3LYP and pob-TZVP). As a consequence, the C_6 parameters for magnesium and silicon are expected to be much lower than in molecular cases, as a result of a much lower atomic polarizability. On the contrary, oxygen polarizability is expected to be much increased, as a result of the negative charge.

Fowler et al.[67] provided an accurate estimation of dispersion coefficients for some metal oxides, showing that C_6^{MgO} and C_6^{MgMg} are about ten and a hundred times smaller, respectively, than C_6^{OO} in MgO, where oxygen has a formal charge of -2 $|e|$.

As a rough approximation, we calculated the surface energies with the B3LYP-D2 functional, with s=1.0 and all C_6 coefficients but C_6^{OO} set to zero. The value used for C_6^{OO}, 35.8 eV Å^6 (named O_{max} in the following paragraphs), corresponds to the estimation reported by Fowler et al.[67] for the O^{2-}-O^{2-} interaction and it is clearly an overestimation of the O-O interaction in olivines. The aim here is to provide an upper limit for the value of surface energy, to compare with the lower limit provided by pure DFT and hybrid functionals. In order to provide a value that is in between these two extremes, the same calculations have been repeated by using C_6^{OO}=17.9 eV Å^6 (O_{min}), corresponding to half the value estimated for the O^{2-}-O^{2-} interaction in MgO.

The last two columns of Table 3 show the results obtained with these two approaches. Notably, the surface stability order remains nearly unchanged. While values obtained with O_{max} represent a very upper limit for the surface energies, it is realistic to hypothesise that the values for this physical quantity fall somewhere in between those obtained with O_{max} and O_{min}. Note that values obtained with O_{min} are quite similar to those obtained with the

PBE0 and PBEsol functionals, whereas values obtained with O_{max} fall in between PBE-D2 and B3LYP-D2.

As a further validation of this approach, bulk properties of forsterite were calculated and compared to those obtained with B3LYP in Table 1 (last three columns). Dielectric constants are nearly the same as those calculated with no dispersion terms. Volumes obtained with the D2 approach are more similar to the experimental values, whereas the agreement on elastic constants and vibrational frequencies worsen when using the standard and the O_{max} parameters. On the contrary, when using the O_{min} parameters, data are nearly of the same quality as those obtained with B3LYP.

Surface Structure

The effect of the choice of DFT functional on the surface structure has been investigated by analysing the distribution of X-O bond lengths and O-X-O bond angles in the atomic layers close to the surface, with X being either Si or Mg. As expected, Si-O bonds are very rigid and their geometry on the surface does not show any major dependence on the functional: in fact, bond lengths are spread over a 0.1 Å wide range of values for each surface orientation, whereas average lengths for different functionals differ by no more than 0.02 Å.

Mg-O distances exhibit a larger flexibility with respect to Si-O bonds, and the effect of functional is correspondingly more pronounced: in this case, lengths span a range about 0.5 Å wide for each surface orientation, and average values for different functionals may differ up to about 0.05 Å. Notably, in the four least stable surface orientations, those Mg sites with very distorted coordination spheres exhibit some dependence on the adopted functional, with Mg-O distances varying up to a few tenths of Å.

Despite being dispersed over ranges of values tens of degrees wide, both O-Si-O and O-Mg-O show average values that are essentially independent on the adopted functional, with differences in the order of 1°.

A full investigation using supercells of all the various surfaces would be computationally expensive with the methods applied in this paper. Since (010) is the most stable surface and therefore where most of the attention will be focused when investigating adsorption and reactivity, we ran supercell calculations to double check that no major surface reconstruction

occurs on this surface.

First, vibrational frequencies were calculated for the primitive cell, using the pob-TZVP basis set and the B3LYP functional. The absence of imaginary modes confirms that the optimized structure is a minimum energy configuration.[68] Then, a 2x2 supercell was fully optimized, to check for the occurrence of a more stable configuration by allowing more degrees of freedom. Both surface energy and structure are the same as in the primitive cell case. This confirms that the primitive cell we used is sufficiently big to represent the surface, which does not undergo any major reconstruction.

CONCLUSIONS

A detailed assessment of the accuracy of several DFT schemes and various basis sets in predicting the surface structure and properties of forsterite is here provided. This work represents a solid background for future investigations of the wide variety of chemical reactions that naturally occur at these surfaces. Two of the considered basis sets were found to be excellent choices. In particular, the use of the most accurate but more time consuming one improves the quality of the results only on those properties that are strongly dependent on the accuracy of the wavefunction (this would include adsorption processes at the surface), whereas convergence on surface structure and stability can be achieved with poorer basis sets, providing that the BSSE correction to the surface energy is appropriately accounted for. Structure and stability of the considered structures did not show major variations with different DFT functionals. However, the least stable surfaces, undergoing major structural arrangements around the surface and sub-surface Mg sites, show some minor differences in Mg-O distances when optimized with different functionals. The effect of including empirical dispersion interactions was investigated. It was demonstrated that with these kinds of materials it is more realistic to consider O-O repulsions as main contributors to the dispersion energy, rather than applying the standard set of C_6 coefficients that would make Mg-Mg, Si-Si and Si-Mg the major contributions. The most stable surface, (010), was shown not to undergo any major reconstruction. he results obtained for the models we propose here are consistent with the data obtained in previous first-principle and force field calculations. A

more detailed investigation could be carried out at a classical level in future work, using the results in this paper as a reference.

ACKNOWLEDGMENTS

This research was supported by Curtin University, through the Curtin Research Fellowship scheme, and by the European Research Council (Starting Grant 2012 n° 307322). Both the Pawsey Supercomputing Centre (Perth) and the Australian National Computational Infrastructure (NCI, Canberra) are acknowledged for the provision of computer time.

	Exp.	B3LYP				B3LYP-D2	B3LYP-D2(O_{max})	B3LYP-D2(O_{min})
		BS1	BS2	BS3	pob-TZVP	pob-TZVP	pob-TZVP	pob-TZVP
Forsterite[a]								
V	289.53	+0.9	+1.9	+1.4	+2.3	-1.4	-0.3	+1.0
C_{11}	330.0	+8.1	+4.0	+3.8	+1.3	+13.8	+17.6	+9.1
C_{22}	200.3	+9.6	+5.6	+6.2	-0.9	+9.7	+8.0	+3.0
C_{33}	236.2	+6.5	+2.2	+2.2	+0.0	+17.7	+9.0	+4.3
C_{44}	67.1	+5.0	-0.5	+1.1	-9.4	+6.4	+9.4	+0.1
C_{55}	81.6	+1.5	+1.0	+1.6	-3.6	+5.9	+10.3	+3.3
C_{66}	81.2	+3.7	+0.0	-0.1	-3.1	+11.7	+13.6	+5.3
C_{12}	66.2	+11.5	+5.2	+5.1	-6.0	+7.5	+10.9	+1.9
C_{13}	68.0	+11.7	+5.9	+5.9	-5.3	+4.0	+9.7	+1.7
C_{23}	72.2	+17.9	+8.0	+9.8	-2.4	+6.1	+6.3	+1.1
ϵ_{xx}	2.77	-12.7	-7.8	-7.2	-3.4	-2.6	-2.7	-3.1
ϵ_{yy}	2.66	-13.9	-9.3	-8.4	-3.9	-3.5	-2.6	-3.6
ϵ_{zz}	2.71	-14.0	-9.2	-8.4	-4.2	-3.6	-2.7	-3.9
$\lvert\bar{\Delta}\nu\rvert$		+18.0	+6.5	+6.9	+5.0	+14.2	+14.9	+7.1
$\Delta\nu_{max}$		+53.5	+21.5	+24.8	+8.3	+34.1	+33.4	+20.0
$\Delta\nu_{min}$		-9.4	-14.1	-13.9	-19.5	-8.15	-12.0	-13.7
t_{SCF}		6.0	9.1	10.3	18.9	[c]	[c]	[c]
(010) surface[b]								
γ	-	1.32	1.23	1.23	1.08	1.51	1.35	1.21
γ_{BSSE}	-	0.94	0.90	0.89	0.93	1.35	1.20	1.06
Si-O_{av1}		1.641	1.648	1.643	1.653	1.650	1.655	1.654
Si-O_{av2}		1.646	1.651	1.646	1.657	1.652	1.659	1.658
Si-O_{max}		1.693	1.701	1.696	1.705	1.703	1.710	1.707
Si-O_{min}		1.606	1.610	1.604	1.616	1.610	1.615	1.615
Mg-O_{max}		2.242	2.257	2.262	2.250	2.203	2.203	2.223
Mg-O_{min}		1.846	1.854	1.855	1.855	1.844	1.847	1.851
t_{SCF}		50.0	63.9	100.8	214.64	[c]	[c]	[c]

Table 1: Bulk properties and surface energy of forsterite as obtained with four basis sets and the B3LYP Hamiltonian. For the pob-TZVP basis set, values obtained with the D2 approach are reported (see text for details).

[a] Percent differences with respect to the experimental values: unit cell volume (V, Å^3) from Ref.[69] ; components of the elastic tensor (C_{ii} and C_{ij}, GPa) from Ref.[70] ; high frequency dielectric tensor (ϵ_{ii}, dimensionless) from Ref.[71]. Mean absolute difference ($\lvert\bar{\Delta}\nu\rvert$, cm^{-1}), maximum and minimum difference ($\Delta\nu_{max}$, $\Delta\nu_{min}$, cm^{-1}) on IR active wavenumbers (ν) with respect to data reported in Ref.[72].

[b] Surface energy (γ, J m^{-2}) and surface energy corrected by BSSE (γ_{BSSE}); average Si-O bond length (Å) for the two independent SiO_4 tetrahedral units on the surface (Si-O_{av1}, Si-O_{av2}); surface Si-O and Mg-O maximum and minimum distance. Time required by one Self Consistent Field step on 64 CPUS (t_{SCF}, s) for the 3D solid and the (010) surface is reported.

[c] The SCF is performed with B3LYP, with dispersion contributions calculated *a posteriori*.

(hkl)	BS2			pob-TZVP		
	γ [32]	γ_{BSSE}	BSSE%	γ	γ_{BSSE}	BSSE%
(010)	1.23	0.90	-27.4	1.08	0.93	-14.3
(120)	1.36	1.10	-19.0	1.20	1.09	-9.2
(101)	1.63	1.21	-25.8	1.39	1.30	-13.4
(001)	1.72	1.29	-25.0	1.54	1.33	-13.8
(111)	1.82	1.32	-27.2	1.60	1.38	-13.8
(021)	1.90	1.38	-27.7	1.73	1.44	-16.7
(110)	2.21	1.62	-26.8	2.01	1.73	-13.7

Table 2: Energy (γ_{BSSE}, J m^{-2}) for the main surfaces of forsterite corrected by the BSSE. Uncorrected values (γ) and the percent difference (BSSE%) between γ_{BSSE} and γ are also reported. Values in this table were obtained by using the B3LYP functional. Similar relative corrections have been obtained with the other functionals.

(hkl)	PBEsol	PBE	PBE0	B3LYP	PBE-D2	B3LYP-D2		
						Grimme[44]	O_{max} [a]	O_{min} [a]
(010)	1.07	0.94	1.06	0.93	1.23	1.35	1.20	1.06
(120)	1.23	1.09	1.22	1.09	1.41	1.51	1.35	1.20
(101)	1.27	1.30	1.44	1.30	1.58	1.79	1.63	1.46
(001)	1.41	1.29	1.45	1.33	1.56	1.72	1.62	1.47
(111)	1.50	1.35	1.52	1.38	1.68	1.87	1.70	1.55
(021)	1.58	1.41	1.59	1.44	1.75	1.95	1.79	1.62
(110)	1.87	1.71	1.88	1.73	1.95	2.14	2.08	1.88

Table 3: Surface energies (γ_{BSSE}, J m^{-2}) for the main crystal surfaces of forsterite, corrected by the BSSE, as obtained with different DFT functionals and the pob-TZVP basis set. [a] s=1.0; $C_6^{OO}(max)$=35.8 eV Å^6; $C_6^{OO}(min)$=17.9 eV Å^6.

References

1. O. Müntener, Geology **38**, 959 (2010).

2. C. Oze and M. Sharma, Geophys. Res. Lett. **32**, L10203 (2005).

3. G. Calas, Elements **9**, 83 (2013).

4. S. Guillot and K. Hattori, Elements **9**, 95 (2013).

5. B. W. Evans, K. Hattori, and A. Baronnet, Elements **9**, 99 (2013).

6. A. Chopelas, Am. Mineral. **76**, 1100 (1991).

7. Y. Noël, M. De La Pierre, L. Maschio, M. Rérat, C. M. Zicovich-Wilson, and R. Dovesi, Int. J. Quantum Chem. **112**, 2098 (2012).

8. F. Belley, E. C. Ferré, F. Martín-Hernández, M. J. Jackson, M. D. Dyar, and E. J. Catlos, Earth Planet. Sci. Lett. **284**, 516 (2009).

9. S. V. Gaisler and B. A. Kolesov, J. Struct. Chem. **48**, 61 (2007).

10. K. E. Kuebler, B. L. Jolliff, A. Wang, and L. A. Haskin, Geochim. Cosmochim. Acta **70**, 6201 (2006).

11. C. Koike, H. Chihara, A. Tsuchiyama, H. Suto, H. Sogawa, and H. Okuda, Astron. Astrophys. **399**, 1101 (2003).

12. D. G. Pearson, F. E. Brenker, F. Nestola, J. McNeill, L. Nasdala, M. T. Hutchison, S. Matveev, K. Mather, G. Silversmit, S. Schmitz, et al., Nature **507**, 221 (2014).

13. P. B. Kelemen and J. Matter, P. Natl. Acad. Sci. USA **105**, 17295 (2008).

14. H. E. King, O. Plümper, and A. Putnis, Environ. Sci. Technol. **44**, 6503 (2010).

15. I. M. Power, S. A. Wilson, and G. M. Dipple, Elements **9**, 115 (2013).

16. T. M. McCollom and J. S. Seewald, Elements **9**, 129 (2013).

17. M. J. Russell, A. J. Hall, and W. Martin, Geobiology **8**, 335 (2010).

18. N. H. de Leeuw, S. C. Parker, C. R. A. Catlow, and G. D. Price, Phys. Chem. Miner. **27**, 332 (2000).

19. N. H. de Leeuw, C. R. A. Catlow, H. E. King, A. Putnis, K. Muralidharan, P. Deymier, M. Stimpfld, and M. J. Draked, Chem. Commun. **46**, 8923 (2010).

20. G. Watson, P. M. Oliver, and S. C. Parker, Phys. Chem. Miner. **25**, 70 (1997).

21. N. H. de Leeuw, S. C. Parker, C. R. A. Catlow, and G. D. Price, Am. Mineral. **85**, 1143 (2000).

22. H. E. King, M. Stimp, P. Deymier, M. J. Drake, C. R. A. Catlow, A. Putnis, and N. de Leeuw, Earth Planet. Sci. Lett. **300**, 11 (2010).

23. K. Muralidharan, P. Deymier, M. Stimpfl, N. H. de Leeuw, and M. J. Drake, Icarus **198**, 400 (2008).

24. S. Kerisit, J. H. Weare, and A. R. Felmy, Geochim. Cosmochim. Acta **84**, 137 (2012).

25. N. H. De Leeuw, J. Phys. Chem. B **105**, 9747 (2001).

26. V. Prigiobbe, A. S. Negreira, and J. Wilcox, J. Phys. Chem. C **117**, 21203 (2013).

27. T. P. M. Coumans, C. R. A. Catlow, and W. A. Brown, Mon. Not. R. Astron. Soc. **393**, 1403 (2009).

28. S. Garcia-Gil, D. T. N. Rougeau, and V. Sidis, J. Phys. Chem. C **117**, 12612 (2013).

29. J. Navarro-Ruiz, P. Ugliengo, A. Rimola, and M. Sodupe, J. Phys. Chem. A **118**, 5866 (2014).

30. J. Navarro-Ruiz, M. Sodupe, P. Ugliengo, and A. Rimola, Phys. Chem. Chem. Phys. **16**, 17447 (2014).

31. C. A. Downing, B. Ahmady, C. R. A. Catlow, and N. H. de Leeuw, Phil. Trans. R. Soc. A **371**, 20110592 (2013).

32. M. Bruno, F. R. Massaro, M. Prencipe, R. Demichelis, M. De La Pierre, and F. Nestola, J. Phys. Chem. C **118**, 2498 (2014).

33. M. F. Peintinger, D. V. Oliveira, and T. Bredow, J. Comput. Chem. **34**, 451 (2013).

34. R. Dovesi, R. Orlando, A. Erba, C. M. Zicovich-Wilson, B. Civalleri, S. Casassa, L. Maschio, M. Ferrabone, M. De La Pierre, P. D'Arco, et al., Int. J. Quantum Chem. **114**, 1287 (2014).

35. F. Pascale, C. M. Zicovich-Wilson, R. Orlando, C. Roetti, P. Ugliengo, and R. Dovesi, J. Phys. Chem. B **109**, 6146 (2005).

36. S. F. Boys and F. Bernardi, Mol. Phys. **19**, 553 (1970).

37. J. P. Perdew, K. Burke, and M. Ernzerhof, Phys. Rev. Lett. **77**, 3865 (1996).

38. J. Perdew, A. Ruzsinsky, G. I. Csonka, O. A. Vydrov, G. E. Scuseria, L. A. Constantin, X. Zhou, and K. Burke, Phys. Rev. Lett. **100**, 136406 (2008).

39. C. Adamo and V. Barone, J. Chem. Phys. **110**, 6158 (1999).

40. A. D. Becke, J. Chem. Phys. **98**, 5648 (1993).

41. C. Lee, W. Yang, and R. G. Parr, Phys. Rev. B **37**, 785 (1988).

42. P. J. Stephens, F. J. Devlin, C. F. Chabalowski, and M. J. Frisch, J. Phys. Chem. **98**, 11623 (1994).

43. S. Grimme, J. Comput. Chem. **25**, 1463 (2004).

44. S. Grimme, J. Comput. Chem. **27**, 1787 (2006).

45. R. Dovesi, V. R. Saunders, C. Roetti, R. Orlando, C. M. Zicovich-Wilson, F. Pascale, B. Civalleri, K. Doll, N. M. Harrison, I. J. Bush, et al., *CRYSTAL 2014 User's Manual* (2014).

46. A. Erba, A. Mahmoud, R. Orlando, and R. Dovesi, Phys. Chem. Miner. **41**, 151 (2014).

47. W. F. Perger, J. Criswell, B. Civalleri, and R. Dovesi, Comput. Phys. Comm. **180**, 1753 (2009).

48. T. J. Hart, Can. Mineral. **16**, 175 (1978).

49. Y. Noël, M. Catti, P. D'Arco, and R. Dovesi, Phys. Chem. Miner. **33**, 383 (2006).

50. R. Demichelis, B. Civalleri, M. Ferrabone, and R. Dovesi, Int. J. Quantum Chem. **110**, 406 (2010).

51. M. De La Pierre, R. Orlando, L. Maschio, K. Doll, P. Ugliengo, and R. Dovesi, J. Comput. Chem. **32**, 1775 (2011).

52. F. Weigend, M. Häser, H. Patzelt, and R. Ahlrichs, Chem. Phys. Lett. **294**, 143 (1998).

53. F. Weigend and R. Ahlrichs, Phys. Chem. Chem. Phys. **7**, 3297 (2005).

54. L. Maschio, B. Kirtman, M. Rérat, R. Orlando, and R. Dovesi, J. Chem. Phys. **139**, 164102 (2013).

55. B. Civalleri and P. Ugliengo, J. Phys. Chem. B **104**, 9491 (2000).

56. B. Civalleri, L. Maschio, P. Ugliengo, and C. M. Zicovich-Wilson, Phys. Chem. Chem. Phys. **12**, 6382 (2010).

57. R. Demichelis, B. Civalleri, P. D'Arco, and R. Dovesi, Int. J. Quantum Chem. **110**, 2260 (2010).

58. D. Tunega, T. Bučko, and A. Zaoui, J. Chem. Phys. **137**, 114105 (2012).

59. R. Demichelis, P. Raiteri, J. D. Gale, and R. Dovesi, J. Phys. Chem. C **117**, 17814 (2013).

60. D. Spagnoli, K. Refson, K. Wright, and J. D. Gale, Phys. Rev. B **81**, 094106 (2010).

61. G. Zhang, W. A. Al-Saidi, E. M. Myshakin, and K. D. Jordan, J. Phys. Chem. C **116**, 17134 (2012).

62. K. Tonigold and A. Groß, J. Chem. Phys. **132**, 224701 (2010).

63. S. Tosoni and J. Sauer, Phys. Chem. Chem. Phys. **12**, 14330 (2010).

64. S. S. Tafreshi, A. Roldan, N. Y. Dzade, and N. H. de Leeuw, Surf. Sci. **622**, 1 (2014).

65. J. Tao and A. M. Rappe, Phys. Rev. Lett. **112**, 106101 (2014).

66. A. Otero-de-la-Roza and E. R. Johnson, J. Chem. Phys. **136**, 174109 (2012).

67. P. W. Fowler, P. J. Knowles, and N. C. Pyper, Mol. Phys. **56**, 83 (1985).

68. H. B. Schlegel, *Geometry optmizaton* (Chichester: Wiley, 1998), vol. 2 of *Encyclopedia of Computational Chemistry*, pp. 1136–1142.

69. A. Kirfel, T. Lippmann, P. Blaha, K. Schwarz, D. F. Cox, K. M. Rosso, and G. V. Gibbs, Phys. Chem. Miner. **32**, 301 (2005).

70. D. G. Isaak, O. L. Anderson, and T. Goto, J. Geophys. Res. **94**, 5895 (1998).

71. W. A. Deer, R. A. Howie, and J. Zussman, *Orthosilicates*, vol. 1A of *Rock forming minerals* (The Geological Society, London, 1982).

72. H. Suto, H. Sogawa, S. Tachibana, C. Koike, H. Karoji, A. Tsuchiyama, H. Chihara, K. Mizutani, J. Akedo, K. Ogiso, et al., Mon. Not. R. Astron. Soc. **370**, 1599 (2006).